Flares from dual jet interactions in supermassive black hole binaries

Eduardo M. Gutiérrez,[1,2,3]★ Luciano Combi,[1,4,5] † Gustavo E. Romero[1,6] and Manuela Campanelli[7]
[1]Instituto Argentino de Radioastronomía (IAR, CCT La Plata, CONICET/CIC), C.C.5, (1984) Villa Elisa, Buenos Aires, Argentina
[2]Institute for Gravitation and the Cosmos, The Pennsylvania State University, University Park PA 16802, USA
[3]Department of Physics, The Pennsylvania State University, University Park PA 16802, USA
[4]Perimeter Institute for Theoretical Physics, Waterloo, Ontario N2L 2Y5, Canada
[5]Department of Physics, University of Guelph, Guelph, Ontario N1G 2W1, Canada
[6]Facultad de Ciencias Astronómicas y Geofísicas, Universidad Nacional de La Plata, Paseo del Bosque s/n, 1900 La Plata, Buenos Aires, Argentina
[7]Center for Computational Relativity and Gravitation, Rochester Institute of Technology, Rochester, NY 14623, USA

Accepted XXX. Received YYY; in original form ZZZ

ABSTRACT

Supermassive black hole binaries (SMBHBs) are natural by-products of galaxy mergers and are expected to be powerful multi-messenger sources. They can be powered by the accretion of matter and shine throughout the electromagnetic spectrum similarly to normal active galactic nuclei (AGNs). Current electromagnetic observatories have good chances to detect and identify these systems in the near future, but we need precise observational indicators to distinguish single AGNs from SMBHBs. In this work, we propose a novel electromagnetic signature from SMBHBs: periodic flares caused by the interaction between the jets launched by the black holes. We investigate close black hole binaries accreting matter from a circumbinary disc and the mini-discs formed around each hole, and launching magnetically-dominated jets in the direction of their spin through the Blandford–Znajeck mechanism. If the spins are slightly inclined, the two jets will encounter each other once per orbit. We argue that this interaction may trigger strong magnetic reconnection events where particles are accelerated and form plasmoids that emit non-thermal radiation. We model the evolution of these particles and calculate the radiative output obtaining spectra and light curves at different wavelengths. We show that these flares can significantly shine in radio, soft X-rays, and γ rays, providing a periodic multi-wavelength electromagnetic signature for SMBHBs.

Key words: black hole mergers – accretion, accretion disks – galaxies:jets – magnetic reconnection – relativistic processes – radiation mechanisms: non-thermal

1 INTRODUCTION

Supermassive black holes (SMBHs) lurk in the centre of most luminous galaxies (Kormendy & Richstone 1995; Magorrian et al. 1998) including some dwarf galaxies (Reines et al. 2013; Mezcua 2017). In the standard cosmological model, galaxies evolve and grow in mass through hierarchical mergers. The observed correlations in the local Universe between black hole masses and bulk properties of their host galaxies suggest they co-evolved during their cosmic history (Kormendy & Ho 2013). SMBH mergers are then a natural byproduct of galaxy evolution.

After two galaxies coalesce, dynamical friction would lead the SMBHs to sink in the galactic remnant and form a 'hard' SMBH binary (SMBHB), reducing the separation from ~ kpc to ~ pc scales (Merritt & Milosavljević 2005). For extreme mass-ratio mergers, dynamical friction does not effectively form a hard binary, leaving a wandering black hole in the galaxy (Kelley et al. 2017). If the SMBHs reach ~ pc scales, dynamical friction ceases to be effective, and the main mechanism to remove angular momentum results from three-body stellar scattering (Begelman et al. 1980; Quinlan 1996). The process remains efficient when sufficient stars with low angular momentum are able to take energy away from the binary (Frank & Rees 1976). Otherwise, the SMBHB system will stall at pc scales; this is known as the 'final parsec' problem (Milosavljević & Merritt 2003). As shown by recent galaxy models, this issue is avoided if the bulge of the galaxy has an asymmetric shape, ensuring a continuous refilling of stars available for scattering Vasiliev et al. (2015). When the system finally reaches a ~ milliparsec separation, the binary evolution is dominated by gravitational radiation, and the black holes eventually merge in less than a Hubble time.

From a theoretical perspective, although we expect SMBHBs to merge after their host galaxies, the process might stall at various stages, leaving wandering black holes or dual AGN systems within the galactic remnant (McWilliams et al. 2014). Similarly, from an observational perspective, SMBHB mergers are neither sufficient nor necessary to explain the observed properties of massive black holes. For instance, linear growth produced by mergers is inadequate to explain quasars at high redshift (Soltan 1982), which instead require exponential mass growth from (super-)Eddington accretion (Small & Blandford 1992). For all these reasons, detecting and characterising SMBHBs as they evolve might help to understand the fundamental relation between galaxies and black holes.

SMBHBs at sub-parsec separations make powerful gravitational wave (GW) sources (Burke-Spolaor et al. 2019). The frequency band of these GWs goes from nanohertz, typical of the inspiral phase of

★ E-mail: emgutierrez@psu.edu
† CITA National Fellow

most massive binaries, to millihertz, typical of the proper merger (chirp). The first detection of low-frequency GWs is expected in the next few years by on-going pulsar timing array (PTA) experiments which aim at measuring the stochastic GW background generated by all the unresolved SMBHB sources (Arzoumanian et al. 2020). Unfortunately, the direct detection of a SMBHB system by GWs will probably have to wait more than a decade, once the planned Laser Interferometer Space Antenna (LISA) mission is on (Mangiagli et al. 2022; Engel et al. 2022), and the capabilities of PTA are improved. Our best chance to find a SMBHB system is through its electromagnetic signatures (Bogdanovic et al. 2021).

Distinguishing normal AGNs from SMBHBs is a hard task. Most of the power in AGNs comes out very near the black hole, in the most internal regions of the thermal disc and the corona. These scales are expected to be, overall, much shorter than the binary separation, so the luminosity of a SMBHB should differ only by small fractions from a normal AGN. Up to this date, there is no confirmed detection of sub-parsec SMBHB sources despite a growing number of candidates (e.g. Valtonen et al. 2008; Dotti et al. 2009; Jiang et al. 2022).

Since we cannot resolve the deep interior of most galaxies, we need robust indicators to separate the emission of normal AGNs, powered by single BHs, from a binary system. Some of the proposals include looking for periodic signals in the light curves (Valtonen et al. 2006; Graham et al. 2015b,a; Liu et al. 2019; Saade et al. 2020) as well as Doppler variations (D'Orazio et al. 2015), broad emission lines shifts (Bogdanović et al. 2009; Dotti et al. 2009), a distinctive "notch" feature in the optical/IR spectrum (Sesana et al. 2011; Roedig et al. 2014), hydro periodicities in the thermal spectrum of mini-discs (Bowen et al. 2019; Combi et al. 2022; Lopez Armengol et al. 2021), and X-ray periodicities (Sesana et al. 2011; Roedig et al. 2014).

In a typical situation, the SMBHB would be immersed in a gas-rich environment. Since we expect this intragalactic matter to have significant amounts of angular momentum, the gas will form a circumbinary disc (CBD). For major mergers, $q > 0.1$, where $q := m_2/m_1$ is the mass ratio and m_i is the mass of the i-th black hole, the torques exerted by the binary give rise to the formation of an eccentric cavity with a mean radius of $\sim 2r_{12}$ (MacFadyen & Milosavljević 2008), where r_{12} is the major semi-axis of the orbit. Although it was initially thought that the binary would decouple at large distances from the CBD, preventing accretion and producing a 'dry' merger (Milosavljević & Phinney 2005), (magneto-)hydro simulations have shown that the accretion rate remains high even at short separations. Within the cavity, mini-discs will form around each BH, being continuously fed by the CBD. For spinning BHs, this material would fill the ergosphere launching jets through the Blandford–Znajeck (BZ) mechanism (Blandford & Znajek 1977).

For sufficiently cold discs and $q > 0.1$, 2D hydro simulations and 3D general relativistic magneto-hydro (GRMHD) simulations show that the inner edge of the CBD develops a non-linear $m = 1$ azimuthal mode, known as the lump, that orbits the binary with a frequency $\Omega_{\rm lump} \approx 0.28\Omega_{\mathcal{B}}$, where $\Omega_{\mathcal{B}}$ is the binary orbital frequency. For this scenario, it was shown that accretion is enhanced when one of the BHs passes near the inner edge of the lump, feeding the correspondent mini-disc at a beat frequency given by $\Omega_{\rm beat} = f_{\mathcal{B}} - \Omega_{\rm lump} \approx 0.72\Omega_{\mathcal{B}}$ (Bowen et al. 2018). At sufficiently short separations, $r_{12} \lesssim 20R_{\rm g}$, where $R_{\rm g} := G(m_1 + m_2)/c^2$, c is the speed of light in vacuum, and G is the gravitational constant, a mini-disc depletes most of its mass before the next accretion event. The system then enters a filling-depleting cycle with a characteristic frequency given by $\Omega_{\rm beat}$, which reflects on the luminosity (Gutiérrez et al. 2022).

If the binary contains rotating black holes, each of them can launch a jet by the BZ mechanism (see Sec. 2.3). In recent years, several simulations have been carried out to study the production of jets in SMBHBs. The first of these considered magnetic fields in vacuum (Palenzuela et al. 2009; Mösta et al. 2010) or under the force-free approximation (Palenzuela et al. 2010a,b; Palenzuela et al. 2010c; Alic et al. 2012; Moesta et al. 2012). These simulations can model what happens if a SMBHB decouples from the CBD but continues to interact with the magnetic field anchored to it. Although these studies indicated that the twisting of the magnetic field lines caused by the SMBHB produces the launching of dual jets in the form of a Poynting flux, their luminosity is low ($\sim 10^{44}$ erg/s for a $M = 10^8$ system) and thus their radiation is probably not detectable (Alic et al. 2012; Moesta et al. 2012).

Ideal GRMHD simulations of SMBHBs accreting on a uniform medium show that the luminosity of dual jets could be much stronger (Giacomazzo et al. 2012; Kelly et al. 2017; Cattorini et al. 2021; Paschalidis et al. 2021a; Combi et al. 2022). Due to the presence of gas accretion, the magnetic field can be amplified by several mechanisms, and the Poynting flux of the jets could increase up to $\sim 10^{48}$ erg/s for a $M = 10^8$ system (Kelley et al. 2017).

The production of jets has also been studied by 3D GRMHD simulations of SMBHBs accreting through a CBD and forming mini-discs (Farris et al. 2012; Gold et al. 2014a,b; Paschalidis et al. 2021b; Combi et al. 2022). These studies also show the formation of two collimated jets. The difference with the uniform plasma scenario is that now the SMBHB decouples from the CBD in the last stages before the merger ($r_{12} \lesssim 10R_{\rm g}$), thus decreasing the accretion rate and the luminosity of the jets. Gold et al. (2014b) also studied the dependence of the intensity of the Poynting flux with the mass-ratio, q, finding that it decreases for decreasing values of q. Therefore, the production of jets is most favourable if the SMBHB system has $q > 0.1$. The spin dependence of BHs in these scenarios was studied by Paschalidis et al. (2021b) and Combi et al. (2022), who also found an increase in the Poynting flux intensity for higher spin values. Additionally, Combi et al. (2022) found that the Poynting flux is modulated with the beat frequency in the same way as the accretion rate. This result indicates that the quasi-periodicity induced by the lump in the luminosity of the mini-discs may also be present in the emission of the jets associated with them.

All the previous work mentioned above considers SMBHBs where the holes have zero spin or aligned/anti-aligned spins with each other and with the angular momentum of the global disc. If the spin of a black hole is misaligned with respect to the angular momentum of the plasma, it will induce a Lense–Thirring (Lense & Thirring 1918) torque on the accretion flow and vice-versa. Because of its viscous stresses, the accretion disc is expected to align with the direction of the BH spin at the inner radii, in what is known as the Bardeen–Petterson mechanism (Bardeen & Petterson 1975; Kumar & Pringle 1985). The occurrence of this effect has been demonstrated in smoothed-particle hydrodynamics (SPH) simulations (Nelson & Papaloizou 2000; Lodato & Pringle 2007; Lodato & Price 2010) and GRMHD simulations (Liska et al. 2019, 2021).

The Bardeen–Peterson mechanism also works in the opposite direction; on longer timescales, it causes the spin of the hole to end up aligning with the angular momentum of the outer disc(Natarajan & Pringle 1998; King et al. 2005; Perego et al. 2009). In the case of SMBHBs, the first studies in this regard indicated that this mechanism does occur between the mini-discs and the BHs, giving rise to the spins aligning with the angular momentum of the CBD in a relatively short time with respect to the evolution of their orbit (Bogdanović et al. 2007; Dotti et al. 2010; Miller & Krolik 2013). Recently, however, it was found that this effect is not sufficient to align the spin of the most massive BH in systems with $q \ll 1$. Fur-

thermore, even if $q \sim 1$, for certain CBD conditions the spins might remain misaligned during the later stages of the inspiral and during the merger (Lodato & Gerosa 2013; Gerosa et al. 2015, 2020; Nealon et al. 2022). In particular, the initial alignment of the mini-disc with the spin of the BH produces itself a 'slowing' effect for the alignment of the spin with the global angular momentum of the CBD (Nealon et al. 2022).

If the binary is instead on a uniform environment, spin misalignment with the orbital angular momentum can also trigger periodicities in the accretion, as demonstrated recently by Cattorini et al. (2021) doing GRMHD simulations of a BH binary near merger; a physical explanation of this phenomena, however, still need further investigation. The final stage of spins just before merger has important implications for the GW emission (Campanelli et al. 2006a) and post-merger kicks (Campanelli et al. 2006b).

Given the discussion above, it is important to understand what sort of electromagnetic emission we get when the spins of the black holes are not aligned. If spins are misaligned and jets are launched along their directions, the jets would interact; furthermore, the interaction would be periodic, with a frequency associated with the orbital motion of the binary system.

In this work, we accept the hypothesis that the interaction between the jets actually occurs periodically and we investigate the possibility that it gives rise to intense periodic flares in different bands of the electromagnetic spectrum. We focus our study on close binary systems in the regime dominated by gravitational wave (GW) emission.

The basic stages of the interaction between the jets in our model are as follows:

- BZ jets are preferentially launched in the direction of the black hole's spin.
- If the spins of the black holes are misaligned, the jets that each BH launches are misaligned too. This implies that both jets must cross each other once per orbit on a quasi-periodic basis.
- BZ jets are usually magnetically dominated near their launching point. Since both jets can have different magnetic field topologies, when they encounter the magnetic field lines must reconnect for one jet to 'pass through' the other.
- In this process, much of the magnetic energy carried by the jets is released and transferred to the plasma.
- If part of this energy goes to accelerated particles, these will cool by synchrotron radiation and synchrotron-self-Compton (SSC), producing electromagnetic emission.

The remaining of the paper is structured as follows. In Section 2, we describe the physical scenario and introduce the main features of the model. This includes the treatment of the electromagnetic emission of the CBD, the mini-discs and the jets during the time they interact. In Section 3, we show the results of the calculation of spectral energy distributions (SEDs) and light curves, exploring the dependence of these products on the variation of the most relevant model parameters. In Section 4, we discuss the limitations of our model and briefly comment on the observational perspectives of the proposed phenomenon. Finally, in Section 5, we present the conclusions of our research.

2 PHYSICAL MODEL

In this section, we describe a semi-analytical model to estimate the electromagnetic radiation produced by accretion discs and interacting jets in SMBHBs at close separations. The accretion structure in a quasi-circular SMBHB approaching the merger typically consists of a CBD and two mini-discs, one around each black hole, which are fed by streams connecting their external edge with the internal border of the CBD. In addition, we assume that each black hole launches a jet via the BZ mechanism in the direction of its spin. If the spin directions of the holes intersect, the jets must also intersect and cross each other at least once per orbital period —twice if the counter-jet is taken into account.

At the point of interaction, the magnetic field topology in each jet will be typically different. In particular, if the field is dominated by its toroidal component and produced by the BZ mechanism, the field lines in each jet have opposite polarities. The collision of a highly magnetised plasma with different topologies is prone to generate current sheets and large-scale magnetic reconnection phenomena. Moreover, if the jets are magnetically dominated, reconnection is needed for them to cross. In this case, the collision event will last until the jets are 'disrupted' when the power released by reconnection becomes comparable to the total power carried by the jet. A fraction of the energy released in the reconnection event can be used for particle acceleration, giving rise to the formation of magnetised blobs filled with particles following a non-thermal energy distribution. These particles will then cool in the magnetic and radiation fields present in the region emitting electromagnetic radiation. Since the collisions between the jets are periodic, so will this emission. In conclusion, these events have the potential to generate periodic flares in different bands of the electromagnetic spectrum. Figure 1 shows a schematic diagram of the system under the situation described above.

Conventions: Non-primed kinematic quantities (p) refer to the laboratory frame, single-primed quantitites (p') refer to the fluid frame, and double-primed quantities (p'') refer to the plasmoid (blob) frame.

2.1 Spacetime associated with the binary system of black holes

Let us consider two supermassive black holes with masses m_i ($i = 1, 2$) and spins $\vec{J}_i = (G\chi_i m_i^2/c)\hat{s}_i$, where χ_i is the normalised dimensionless spin and $\hat{s}_i$ is a unit vector. Let us assume that the black holes form a binary system and follow circular orbits with a separation $r_{12}(t_0)$ at time $t = t_0$. We consider that the system has reached a stage where the emission of GWs is efficient and dominates the evolution of the orbit, $r_{12} \lesssim 10^3 R_g$. Furthermore, we assume that the orbit evolves slowly, through quasi-circular orbits of decreasing radius. At 1st post-Newtonian order, the separation of the black holes evolves as (Peters 1964)

$$r_{12}(t) = r_{12}(t_0)\left(1 - \frac{t}{t_c}\right)^{1/4} \tag{1}$$

where t_c denotes the coalescence timescale, which is defined as

$$t_c = \frac{2}{256}\frac{c^5}{G^3}\frac{r_{12}(t_0)^4}{M^2\mu}, \tag{2}$$

and $\mu := m_1 m_2/M$ denotes the reduced mass of the system. In this approximation, the orbital frequency of the binary system is given by the Keplerian value:

$$\Omega_{\mathcal{B}}(t) = \frac{c}{R_g}\left(\frac{R_g}{r_{12}(t)}\right)^3. \tag{3}$$

2.2 Circumbinary disc and mini-discs

We assume that the SMBHB is located in an environment with enough gas for a CBD to form. For mass ratios close to unity, the CBD develops a slightly eccentric cavity of mean radius $\sim 2r_{12}(t)$ (Noble

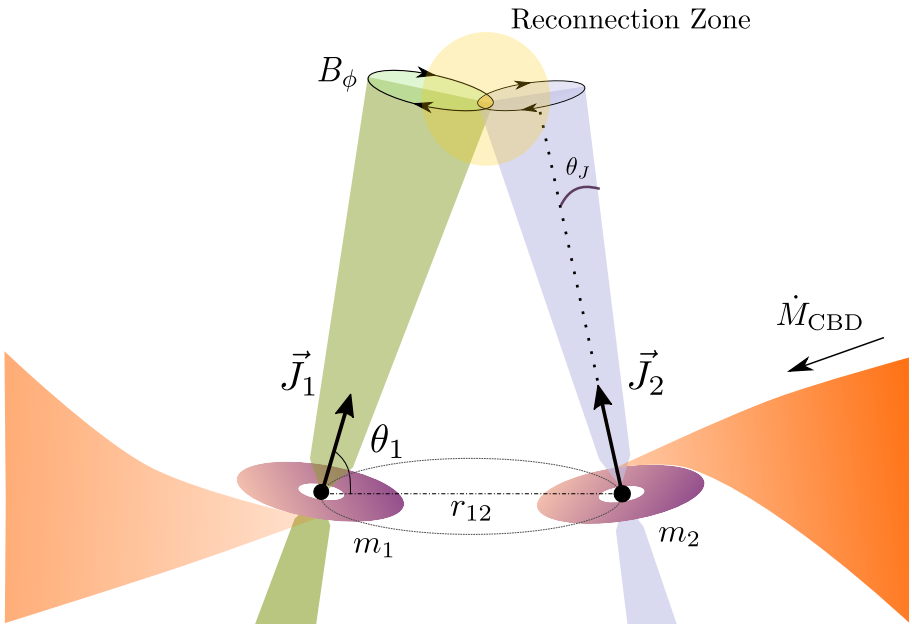

Figure 1. Schematic diagram of an accreting SMBHB with misaligned and partially opposed spins. In the image, the mini-discs, jets, and CBD are shown (along with the streams through which the mini-discs receive matter). The toroidal components of the magnetic field in both jets have opposite polarities and when they collide they give rise to a 'reconnection zone'.

et al. 2021), and accretion into the cavity occurs mainly through thin streams that break off from the inner edge of the CBD. This gas forms mini-discs around each black hole.

For sufficiently cold discs and values of $q > 0.1$, the inner edge of the CBD develops a non-linear $m = 1$ mode, the lump, which orbits the binary at a frequency $\Omega_{\rm lump} \approx 0.28\Omega_{\mathcal{B}}$. For this scenario, accretion occurs primarily when one of the black holes passes close to the inner edge of the lump, feeding the corresponding mini-disc in a quasi-periodic fashion with a beat frequency given by $\Omega_{\rm beat} = \Omega_{\mathcal{B}} - \Omega_{\rm lump} \approx 0.72\Omega_{\mathcal{B}}$ (Bowen et al. 2018; Bowen et al. 2019).

The mini-disc dynamics essentially depends on the relationship between their truncation radius $r_{\rm trunc}$, where tidal effects by the companion hole prevent the formation of stable orbits, and the radius of the ISCO, $r_{\rm ISCO}$, which depends strongly on the spin of the hole (Gold et al. 2014c; Bowen et al. 2019). When $r_{{\rm trunc},i}/r_{\rm ISCO,i} \approx O(1)$, the inflow time of matter in the mini-discs becomes shorter than the beat period, resulting in a filling-and-depleting cycle in which one mini-disc gains matter when passes close to the lump while the other depletes almost completely. At the maximum of this cycle, the receiving mini-disc can have up to 75% of the total mass (for non-rotating black holes) in the cavity. In order to model this effect, we parameterise the accretion rate on each mini-disc as a function of time. Assuming high spins and mass-ratio close to one, the accretion rate in the mini-discs is

$$\dot{m}_{{\rm md},1}(t) = \left\{\frac{1}{2} + \frac{10R_{\rm g}}{r_{12}(t)}\left[\cos^4\left(\frac{\Omega_{\rm beat}}{2}t\right) - 0.36\right]\right\}\dot{M}_{\rm CBD}, \tag{4}$$

$$\dot{m}_{{\rm md},2}(t) = \dot{m}_{{\rm md},1}(t - T_{\rm beat}/2), \tag{5}$$

where $T_{\rm beat} := 2\pi/\Omega_{\rm beat}$ is the period of one filling/depleting cycle and $\dot{M}_{\rm CBD}$ is the (constant) accretion rate in the CBD. The function above reproduces accurately both the cycle and the fact that at large separations the truncation radius of the mini-disc becomes large and the accretion rate becomes stationary. This is shown in Figure 2 for two values of r_{12}.

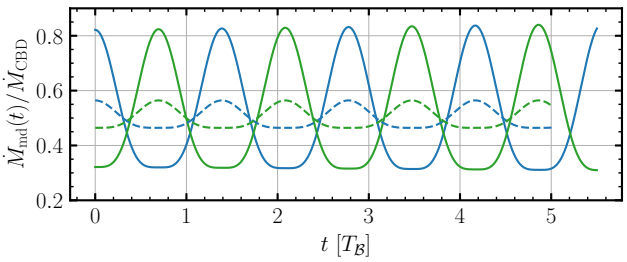

Figure 2. Mini-discs' total accretion rate as a function of time for two values of the black hole separation: *solid lines:* $r_{12} = 20R_{\rm g}$; *dashed lines:* $r_{12} = 100R_{\rm g}$. The time is normalised to the period that corresponds to each separation.

2.2.1 *Electromagnetic emission*

We model the CBD as a Shakura–Sunyaev disc (SSD, Shakura & Sunyaev 1973) onto a black hole of mass $M = m_1 + m_2$ and accretion rate $\dot{M}_{\rm CBD}$, extending from $2r_{12}(t)$ up to $1000R_{\rm g}$. We consider that the dissipation does not vanish at the inner edge of the disc but at the radius of the fictitious ISCO of the binary, $6R_{\rm g}$. Gutiérrez et al. (2022) have shown that this approximation provides a good agreement with the spectrum that results from more detailed numerical simulations. The SSD model provides the effective temperature at each radius. Assuming that the disc radiates a blackbody spectrum, the spectral flux of a CBD for a source located at a luminosity distance d_L is

$$F_{\nu_{\rm o}}^{\rm (CBD)}(t) = \cos i\,\frac{(1+z)}{d_{\rm L}^2}\int_{2r_{12}(t)}^{1000R_{\rm g}} 2\pi r dr B_{\nu_{\rm e}}\left[T_{\rm eff}(r)\right], \tag{6}$$

where i is the inclination of the line of sight of the observer with respect to the angular momentum of the disc, $B_{\nu_{\rm e}}$ is the Planck function, $T_{\rm eff}(r) = [D(r)/\sigma]^{1/4}$, $D(r)$ is the energy dissipated per unit area in an SSD, σ is the Stefan–Boltzmann constant, $\nu_{\rm o} = \nu_{\rm e}/(1+z)$ is the observed frequency, $\nu_{\rm e}$ is the emitted frequency, and we have included the correction due to the cosmological redshift of the source, z.

Mini-discs are much more dynamic and therefore more complex to model than the CBD. Besides the periodic variation in their accretion rate, at short binary separations, a significant part of the matter that falls onto them from the inner edge of the CBD has a low specific angular momentum and pulls directly onto the hole without forming a circular orbit (Combi et al. 2022); thus, this fraction of matter suffers little dissipation and cooling (Gutiérrez et al. 2022). This effect would be more important for short separations, whereas when the separation between the holes is sufficiently large, the mini-discs will resemble normal discs in single black hole systems. To account for this effect, we define for each mini-disc an effective accretion rate $\dot{m}_{\rm eff} < \dot{m}_{\rm md}$ as

$$\dot{m}_{\rm eff}(t) = \dot{m}_{\rm md}(t)\left[\frac{1-(r_{\rm in}/r_{12})^s}{1-(r_{\rm in}/r_{\rm out})^s}\right] \times H[r_{12}(t); r_{\rm in}, r_{\rm out}], \tag{7}$$

where $s = 0.2$, $r_{\rm in} = 10R_{\rm g}$, $r_{\rm out} = 500R_{\rm g}$, and H is the Heaviside step function.

In addition, similarly to AGNs, a fraction of the emitting matter is expected to be in the form of a hot, optically thin, inflated corona located above and below the mini-disc. Following the approach of d'Ascoli et al. (2018) and Gutiérrez et al. (2022), we assume that the mini-disc spectrum consists of two components: a thermal multi-temperature blackbody emitted by the cold disc and an extended power law with an exponential cutoff in hard X-rays emitted by the hot corona.

We model the cold thin part of the ith mini-disc as a Novikov–Thorne (NT) disc (since mini-discs extend down to the ISCO of the black holes, it is more accurate to consider the relativistic solution) on a black hole of mass m_i and accretion rate $\dot{m}_{{\rm eff},i}$. We consider that each mini-disc extends from $r_{{\rm ISCO},i}$ to the truncation radius $r_{{\rm trunc},i}$ and its angular momentum is aligned with the spin of the black hole. Since each mini-disc is anchored to one of the black holes and these are moving very fast, we must take into account the global effect of beaming and the relativistic Doppler shift caused by the orbital motion. Then the observed spectral flux of each mini-disc is

$$F^{\rm (md)}_{\nu_{\rm o}}(t) = \mathcal{D}^3_{\rm md}(t)\cos i_{\rm md}\frac{(1+z)}{d_{\rm L}^2}\times \int_{r_{\rm ISCO}}^{r_{\rm trunc}(t)} 2\pi r dr\left[1+z_{\rm g}(r)\right]^{-3} B_{\nu_{\rm e}}\left[T_{\rm eff}(r,t)\right], \tag{8}$$

where, now,

$$\nu_{\rm o} = \mathcal{D}_{\rm md}(t)\nu'(r)/(1+z), \text{ with } \nu'(r) = \nu_{\rm e}/[1+z_{\rm g}(r)], \tag{9}$$

$\mathcal{D}_{\rm md}(t) := \left[\Gamma_{\rm md}\left(1-\vec{\beta}_{\rm md}\cdot\hat{o}\right)\right]^{-1}$ is the Doppler factor, $\beta_{\rm md} := v_{{\rm md},i}/c$ is the normalised speed of the mini-disc (or associated black hole) and $i_{\rm md} = \arccos(\hat{s}_i\cdot\hat{o})$ is the angle between the normal to the mini-disc, $\hat{s}_i$, and the direction of the line of sight, $\hat{o}$. It is worth noting that if the spins are not perfectly aligned with the orbital angular momentum, $i \neq i_{\rm md}$ in general. In Eq. 8, we have also included the relativistic effects due to the gravitational redshift, $z_{\rm g}$.

Finally, we model the corona as a homogeneous spherical plasma with temperature $T_{\rm c}$ and radiative efficiency $\eta_{\rm c}$, which emits an effective power-law spectrum with an exponential cutoff. This spectrum is the result of the Comptonisation of the soft photon spectrum from the thin disc. The coronal spectral flux is

$$F^{\rm (c)}_{\nu_{\rm o}}(t) = \mathcal{D}^3_{\rm md}(t)\frac{(1+z)}{4\pi d_L^2}\frac{L_{\rm c}}{\pi}\frac{h}{k_{\rm B}T_{\rm c}}\left(\frac{h\nu_{\rm e}}{k_{\rm B}T_{\rm c}}\right)^{-\alpha}\exp\left(-\frac{h\nu_{\rm e}}{k_{\rm B}T_{\rm c}}\right), \tag{10}$$

where $L_{\rm c} := \eta_{\rm c}\dot{m}_{\rm eff}c^2$ is the bolometric luminosity of the corona.

2.3 Jets

We assume that each mini-disc launches a jet in the direction of the black hole's spin via the BZ mechanism. We assume that the power of each jet is proportional to the total accretion power onto the corresponding black hole (Falcke & Biermann 1995):

$$L_{{\rm j},i} = \eta_{\rm j}\dot{m}_{{\rm md},i}c^2. \tag{11}$$

In what follows, we set $\eta_{\rm j} = 0.1$ which is compatible with recent GRMHD simulations of SMBHB's mini-discs (Paschalidis et al. 2021b; Combi et al. 2022). We assume a quasi-parabolic geometry for the jets and express the radius of its cross-section as

$$r(\tilde{z}) = r_0\left[1+(\tilde{z}/z_0)^{\alpha}\right], \tag{12}$$

where $\tilde{z}$ is the vertical coordinate along the jet axis and we take $\alpha = 0.6$.

If the specific enthalpy of the jet, h'[1], is ~ 1, i.e., if the jet is cold, the Lorentz factor $\Gamma_{\rm j}$ is related to its magnetisation through the Bernoulli equation:

$$\mu := \Gamma_{\rm j}(\sigma'+1), \tag{13}$$

where $\sigma' := B'^2/(4\pi\rho' c^2)$ is the magnetisation parameter, B' is the strength of the magnetic field, ρ' is the rest-mass density, and μ is the total energy flux per unit of rest-mass energy flux through a cross-section of the jet, which is constant along it. For the scales we are interested in, we can assume that the magnetisation is constant and, therefore, so is the Lorentz factor.

Given the modulation of the accretion rate in the mini-discs, Eq. 11 implies that the power of the jet will also be periodically modulated; this is compatible with findings in the GRMHD simulations performed by Combi et al. (2022). This modulation should occur with a delay with respect to the discs; at an instant of time t and at a height $\tilde{z}$ above the jet, its power is

$$L_{\rm j}(t,\tilde{z}) = \eta_{\rm j}\dot{m}(t_{\rm ret})c^2, \tag{14}$$

where $t_{\rm ret} := t - \tilde{z}/v_{\rm j}$ and $v_{\rm j} := c(1-\Gamma_{\rm j}^{-2})^{1/2}$ is the (constant) speed of the jet.

We can express the jet power at a given height $\tilde{z}$ as

$$L_{\rm j} = \Gamma_{\rm j}^2 v_{\rm j}\pi r(\tilde{z})^2\rho' c^2\left(\sigma'+1\right). \tag{15}$$

From Eq. 15 and using the definition of σ', we can obtain the comoving magnetic field at time t and height $\tilde{z}$ as

$$B'(t,\tilde{z}) = \frac{2}{\Gamma_{\rm j} r}\sqrt{\frac{L_{\rm j}(t,\tilde{z})}{v_{\rm j}}\left(\frac{\sigma'}{\sigma'+1}\right)}. \tag{16}$$

Therefore, the magnetic field varies with time and height following the modulation of the jet power.

2.4 Interaction between the two jets

Unless the black holes' spins are perfectly aligned[2], the two jets will encounter each other once per orbit[3]. When the edges of the

[1] The specific enthalpy is defined as $h' = 1 + (p'+\epsilon')/(\rho' c^2)$, where p' and ϵ' are the pressure and internal energy of the particles in the jet.

[2] This case is interesting in itself, since the jets would be in constant contact, which may trigger plasma instabilities and magnetic reconnection events on timescales directly related to the microphysical properties of the plasma.

[3] The counter-jets will also collide with the same frequency and out of phase with the jets. However, we will neglect the emission of counter-jets since it will be de-beamed.

two jets approach and encounter, regions of plasma with potentially opposite magnetic polarities converge at high speeds. This situation is highly favourable for the formation of current sheets and large-scale magnetic reconnection regions. Moreover, relativistic BZ jets are magnetically dominated ($\sigma' > 1$) near its base. This makes them *magnetically rigid*, and so they cannot cross each other unless a significant part of the global magnetic field reconnects. It is then reasonable to expect large amounts of energy to be released in these events.

Numerous particle-in-cell (PIC) simulations show that, under similar conditions, magnetic reconnection results in the formation of a series of magnetised plasmoids of different sizes along the current sheet (Samtaney et al. 2009; Uzdensky et al. 2010; Sironi & Spitkovsky 2014; Sironi et al. 2016; Petropoulou et al. 2016, 2018). These plasmoids travel along the current sheet and grow in size while keeping their density and magnetic induction field constant (Sironi et al. 2016). In the reference frame of a given plasmoid, hereafter indicated with double primes ($''$), particles are accelerated forming a (non-thermal) power law distribution approximately isotropic (Zenitani & Hoshino 2001; Sironi & Spitkovsky 2011, 2014; Petropoulou et al. 2019). The spectral index of the distribution, p, is directly related to the value of the magnetisation parameter in the non-reconnected plasma, i.e. in the jet, being lower (harder spectra) for higher magnetisation values (Sironi & Spitkovsky 2014; Sironi et al. 2016; Werner et al. 2016; Guo et al. 2014, 2015, 2016, 2021; Petropoulou et al. 2019).

For our model, we will simply assume that two large magnetised blobs are formed in the collision event, one in each jet, moving along current sheets at the contact surface of the two jets. We assume that the collision is practically spatially stationary until the reconnected magnetic energy becomes comparable to the energy carried by any of the jets. At this point, one or both of the jets break off and cross each other. If the magnetic flux built around the holes is not catastrophically disrupted, we can assume that after crossing the jets will form again in a timescale shorter than the orbital period.

The duration of the interaction between the jets can be estimated from purely geometric arguments as $t_{\rm dur} \approx 2[r_{\rm j}^{(1)} + r_{\rm j}^{(2)}]/(2v_{\rm orb})$, where $r_{\rm j}^{(i)}$ is the radius of the ith jet at the height of the collision. Nevertheless, the jets will likely disrupt on a shorter timescale $t_{\rm break}$, when the reconnected energy per unit time, $L_{\rm rec}$, becomes comparable to the power carried by the jet. If the jet power is distributed homogeneously on a given cross-section, $L_{\rm rec}$ will be proportional to the volume of the intersected region. If $r_{\rm j,1} < r_{\rm j,2}$, this volume grows approximately linearly between $t = 0$ and $t_1 = r_{\rm j,1}/(r_{\rm j,1}+r_{\rm j,2})\times t_{\rm dur}$, remains constant between t_1 and $t_2 = r_{\rm j,2}/(r_{\rm j,1}+r_{\rm j,2})\times t_{\rm dur}$, and then decreases linearly between t_2 and $t_{\rm dur}$. Let us assume that the jets break up when $L_{\rm rec}$ is a 10% of the magnetic power of the weaker jet, $L_B^{(1)}$. Then, we set $t_{\rm break} = 0.1t_1$. Furthermore, we consider that when the edges of the jets encounter at a time $t_{\rm coll}$, the reconnected fractional power grows very rapidly in the intersected region with a time scale $t_{\rm rise} \ll t_{\rm dur}$.

Defining $\xi := (t - t_{\rm coll})/t_{\rm dur}$, we propose a simple parameterisation of these two effects and express the fractional power released at the normalised time ξ in each jet as

$$\frac{L_{\rm rec}(\xi)}{L_B^{(1)}(t_{\rm coll}+\xi t_{\rm dur}, \tilde{z}_{\rm coll})} = \mathcal{A}(\xi)\mathcal{B}(\xi;\xi_{\rm rise},\xi_{\rm break}), \tag{17}$$

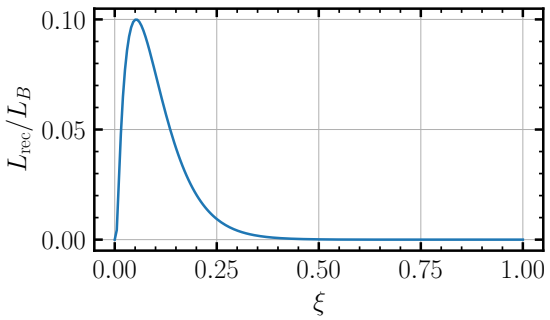

Figure 3. Reconnected energy as a function of the time during a given jet-jet collision.

where

$$\mathcal{A}(\xi) = \begin{cases} \xi/t_1, & \text{if } 0 < \xi < \xi_1 \\ 1, & \text{si } \xi_1 \le \xi \le \xi_2 \\ (1-\xi)/(1-\xi_2), & \text{if } \xi_2 < \xi \le 1 \\ 0, & \text{in other case,} \end{cases} \tag{18}$$

models the volume fraction of the intersection region and thus the strength of the magnetic field in the reconnection region, with $\xi_{1,2} := t_{1,2}/t_{\rm dur}$, and

$$\mathcal{B}(\xi) = \begin{cases} \mathcal{B}_0 \left(1 - e^{-\xi/\xi_{\rm rise}}\right) e^{-\xi/\xi_{\rm break}}, & \text{if } 0 < \xi \le 1 \\ 0, & \text{in other case,} \end{cases} \tag{19}$$

is a *fast-rise/exponential-decay* function that phenomenologically models the fast growth of the reconnected power and the decay after the jets break. Here, $\mathcal{B}_0$ is a constant such that $\mathcal{A}(\xi)\mathcal{B}(\xi)$ is normalised to 0.1.

From the total reconnect power at a given normalised time ξ during the collision, we assume that a constant fraction $f_{\rm rec} \sim 0.5 f_{\rm e}\sigma'/(\sigma'+2)$[4] is transferred to the accelerated particles (Sironi et al. 2015), which are injected with a power-law spectrum in the comoving frame of the plasmoid:

$$Q''(\gamma'';\xi) = Q_0''(\xi)\gamma''^{-p} H[\gamma'';\gamma''_{\rm min},\gamma''_{\rm max}]. \tag{20}$$

Here, $H[x;x_1,x_2]$ is the Heaviside function and $Q_0''(\xi)$ is determined by the condition that the power per unit volume injected into non-thermal particles at time ξ is $f_{\rm rec}L_{\rm rec}(\xi)$ in the laboratory frame.

The minimum and maximum Lorentz factor of the distribution depends on whether $p > 2$ (soft spectrum) or $p < 2$ (hard spectrum). For a proton-electron plasma with $p > 2$, the average energy per particle available for dissipation is $\sim \sigma'/2$ and the minimum Lorentz factor is

$$\gamma''_{\rm min} \approx \frac{f_{\rm rec}\sigma'}{2N_\pm}\frac{(p-2)\,m_{\rm p}}{(p-1)\,m_{\rm e}}, \tag{21}$$

where $m_{\rm p}$ and $m_{\rm e}$ are the mass of the proton and electron, respectively, and $N_\pm \ll m_{\rm p}/m_{\rm e}$ is the multiplicity of pairs. In low pair multiplicity scenarios, $f_{\rm rec}$ depends on the magnetisation and is ≈ 0.15 for $\sigma' \sim 3$, reaching a value of $f_{\rm rec} \approx 0.25$ for $\sigma' \approx 10$. If, on the contrary, $N_\pm \gg 1$, the pairs get most of the dissipated magnetic energy and $f_{\rm rec} \sim 0.5$.

The maximum Lorentz factor in this case is limited by the balance between the acceleration and cooling rates. If we write the acceleration timescale as

$$t''_{\rm acc} = \frac{\gamma'' m_{\rm e} c \epsilon_{\rm acc}}{eB''}, \tag{22}$$

[4] PIC simulations find $f_{\rm e} \sim 1$ for electron-positron plasmas and $f_{\rm e} \sim 0.5$ for electron-proton plasmas (Sironi & Spitkovsky 2014; Melzani et al. 2014).

where e is the charge of the electron and $\epsilon_{\rm acc}$ is the number of cycles an electron undergoes before being injected into the non-thermal population, and we assume that the dominant cooling process in the blob is synchrotron radiation, the maximum Lorentz factor is

$$\gamma''_{\rm max} = \sqrt{\frac{6\pi e}{\epsilon_{\rm acc}\sigma_{\rm T} B''}}, \tag{23}$$

where $\sigma_{\rm T}$ is the Thomson cross section.

On the other hand, if $p < 2$, which is the case for $\sigma' > 10$, most of the energy is carried by the higher energy particles, and $\gamma''_{\rm max}$ is limited by σ'. More precisely, considering that the average energy per particle cannot exceed $(\sigma'+1)m_{\rm p}c^2$ (Sironi & Spitkovsky 2014; Guo et al. 2015; Werner et al. 2016), the maximum Lorentz factor becomes

$$\gamma''_{\rm max} = \left[\frac{f_{\rm rec}\sigma'}{2N_{\pm}}\frac{(2-p)\,m_{\rm p}}{(p-1)\,m_{\rm e}}\right]^{1/(2-p)}, \tag{24}$$

and $\gamma_{\rm min}$ is not important; in this case, we set $\gamma_{\rm min} = 2$.

The acceleration and cooling timescales of the particles are much shorter than the duration of the event:

$$t_{\rm acc} \lesssim t_{\rm cool} \ll t_{\rm dur}. \tag{25}$$

Therefore, we can assume that the particle distribution stabilises very quickly and, at each time, we can solve a steady-state transport equation:

$$\frac{d}{d\gamma''}\left[\dot{\gamma}''|_{\rm loss} N''(\gamma'';\xi)\right] + \frac{N''(\gamma'';\xi)}{t'_{\rm esc}} = Q''(\gamma'';\xi), \tag{26}$$

where $\dot{\gamma}''|_{\rm loss} = \dot{\gamma}''|_{\rm sync} + \dot{\gamma}''|_{\rm SSC}$.

Once we obtain the stationary particle distribution $N''(\gamma'',\xi)$ in the comoving frame of the plasmoid at each instant ξ, we calculate the emissivities by synchrotron and SSC, as well as the absorption coefficients by synchrotron-self-absorption (SSA) and by the photo-pair creation process ($\gamma\gamma \rightarrow e^+e^-$).

Finally, the observed spectral flux on Earth at time $t_{\rm o} = (1+z)(t_{\rm coll} + \xi t_{\rm dur})$ is (Dermer & Menon 2009)

$$\nu_{\rm o} F_{\nu_{\rm o}}(t_{\rm o}) = \left(\frac{3u(\tau'')}{\tau''}\right)\frac{\mathcal{D}_{\rm p}^4 V''}{d_L^2}\nu'' j''_{\nu''}(t_{\rm e}), \tag{27}$$

where $\nu_{\rm o} = \mathcal{D}_{\rm p}\nu''/(1+z)$, and

$$u(\tau'') = \frac{1}{2} + \frac{e^{-\tau''}}{\tau''} - \frac{\left(1-e^{-\tau''}\right)}{\tau''^2}, \tag{28}$$

where $\tau'' = 2R''(\kappa_{\rm SSA} + \kappa_{\gamma\gamma})$ is the total internal optical depth.

The Doppler factor of the plasmoid, $\mathcal{D}_{\rm p}$, depends on the direction and the Lorentz factor with which it moves in the comoving frame of the jet. For simplicity, we will assume that most of the emission is produced by slightly relativistic plasmoids (in the jet reference frame) and take $\Gamma'_{\rm p} \approx 1$ and so, $K'' \equiv K'$ and

$$\mathcal{D}_{\rm p} \simeq \mathcal{D}_{\rm j} = \left[\Gamma_{\rm j}\left(1 - \beta_{\rm j}\cos\alpha_{\rm j}\right)\right]^{-1}. \tag{29}$$

3 RESULTS

The general scenario described above applies to a large number of configurations with different geometrical and physical parameters. The main parameters of the model are the (initial) separation of the black holes, r_{12}; the total mass, M; the mass ratio, q; the black hole spin vectors, $\vec{J}_i$; the accretion rate in the CBD, $\dot{M}_{\rm CBD}$; the luminosity of the jet, $L_{\rm j}$ (or, equivalently, the efficiency $\eta_{\rm j}$), the Lorentz factor of the jet, $\Gamma_{\rm j}$, the magnetisation, σ'; and the line of sight inclination, i. See Table 1 for the numerical values of the parameters we use in our fiducial model.

Table 1. Parameters of the fiducial model.

Parameter	Symbol	Fiducial Value
m_1, m_2	Masses of the black holes	$10^8 M_\odot, 10^8 M_\odot$
r_{12}	Binary Separation	$30\ R_{\rm g}$
χ_1, χ_2	Norm. spins of the black holes	0.9, 0.9
θ_1, θ_2	Spin Inclinations	10°,10°
d_L	Luminosity distance	1 Gpc
r_0, z_0	Jet quasi-parabolic geometry	$2\ R_{\rm g}$
i	Viewing Angle	0°
$\dot{M}_{\rm CBD}$	Accretion rate of the CBD	$\dot{M}_{\rm Edd}$
$\eta_{\rm jet}$	Jet efficiency	0.1
$\Gamma_{\rm j}$	Jet Lorentz factor	5
σ'	Com. Magnetisation	10
p	Spectral Index	2.1
$f_{\rm rec}$	Reconnection energy fraction	0.25
$N_{\pm}$	Multiplicity of pairs	1

The CBD emits a non-periodic thermal spectrum that only varies secularly as the binary orbit shrinks due to GW emission. In contrast, each mini-disc emits a variable coronal + thermal spectrum that oscillates periodically due to two effects: the modulation of the accretion rate by the lump, with a frequency $f_{\rm beat} \approx 0.7 f_{\mathcal{B}}$, and the relativistic beaming due to the fast orbital motion of the black holes, with a frequency $f = f_{\mathcal{B}}$. Furthermore, the luminosity of the mini-discs decays secularly due to the decrease in both $r_{\rm trunc}(t)$ and the fraction of the accretion rate that thermalises in the disc (Eq. 7). The emission of the jets consists of periodic flares at a rate of once per orbit, when the collision between both jets occurs. These flares are, in turn, modulated by the same effects that affect the mini-discs. This modulation in the emission of the jets would occur with a phase shift of $\Delta t \approx \tilde{z}/v_{\rm j} - \cos\omega\tilde{z}/c$ with respect to the mini-disc emission, where ω is the angle between the direction of the jet and the line of sight.

In what follows, we explore the temporal and spectral dependence of the emission of the CBD + mini-discs + jets system for different scenarios.

3.1 Spectral energy distributions

First, we define a fiducial model by setting $m_1 = m_2 = 10^8 M_\odot$, $\dot{M}_{\rm CBD} = \dot{M}_{\rm Edd}$, $\eta_{\rm jet} = 0.1$, $\chi_1 = \chi_2 = 0.9$, $z_0 = r_0 = 2R_{\rm g}$, $\Gamma_{\rm j} = 5$, $q = 1$, $d_L = 1$Gpc. Then, we explore how the SED varies at the point of maximum emission of the jet flare for different values of σ', spin inclination, θ_i, i, r_{12} and M. We define our fiducial microphysical parameters setting $\sigma' = 10$, $p = 2.1$, $f_{\rm rec} = 0.25$, $N_{\pm} = 1$, $r_{12} = 30R_{\rm g}$, $i = 0°$ and spins tilted 10° with respect to the orbital angular momentum and facing azimuthally. Figure 4 shows the SED of the fiducial model at the time of maximum emission of the jets. The spectrum of the CBD and of the mini-discs are similar to those obtained in Gutiérrez et al. (2022), although here the mini-discs are brighter. This is due to two reasons: a) we have considered higher spins, $\chi_1 = \chi_2 = 0.9$, so the discs are intrinsically more massive, hotter, and thus brighter, and b) the separation of the black holes is higher and we have assumed (see Eq. 7) that mini-discs have a larger fraction of their mass thermalised at larger separations. The

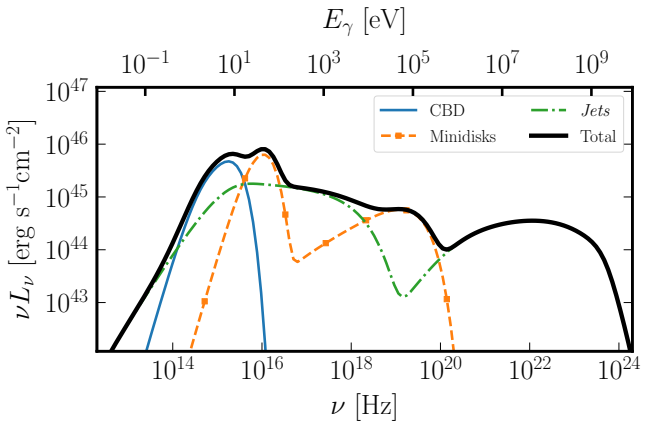

Figure 4. Spectral energy distribution of a SMBHB at the maximum emission of the jets for the fiducial model with $m_1 = m_2 = 10^8 M_\odot$, $q = 1$, $\dot{M}_{\rm CBD} = \dot{M}_{\rm Edd}$, $\sigma' = 10$, $p = 2.1$, $f_{\rm rec} = 0.25$, $N_\pm = 1$, $r_{12} = 30R_{\rm g}$, $i = 0°$ and $\theta_1 = \theta_2 = 10°$ and facing azimuthally. The different contributions to the SED are shown in different line-styles and colours: CBD (solid blue line), mini-discs (orange dashed line), jets (green dashed and dotted line).

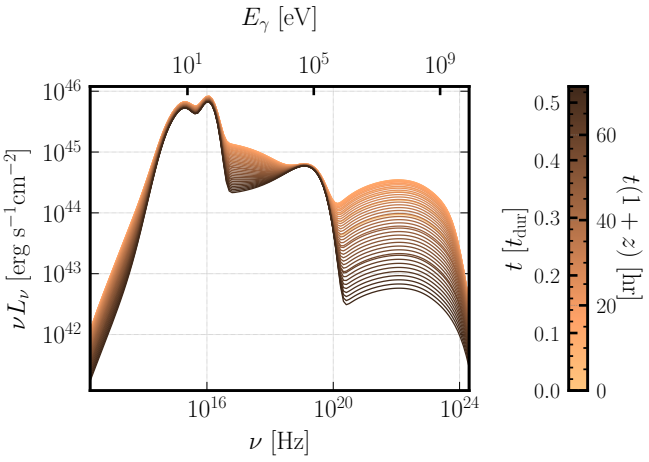

Figure 5. Spectral distribution of energy of the SMBHB for different times during a flash produced by the collision of these jets. The parameters correspond to the values of the fiducial model. In the colour bar, $t_{\rm dur}$ is the total duration of the event.

corona emits 10% of the luminosity with a spectrum identical to that of the simulations in Gutiérrez et al. (2022). The novelty in the SED here is in the emission of the jets; more precisely, of the collision region of these. This spectrum consists of two broad bumps caused by synchrotron emission, the first, peaking at frequency $\nu \sim 10^{16}$Hz, and by SSC, the second, with maximum at an energy of $\sim$ 100MeV.

In Figure 5, we show how the SED of the fiducial model changes during a flare. The increase in luminosity from the stationary value is very fast, so it is hardly noticeable on the graph. The different curves with increasingly darker colours correspond to the decay phase of the flash. On the other hand, it can also be seen that the mini-discs practically do not vary during the entire flash. For the value of the total mass of $M = 2 \times 10^8 M_\odot$ and the redshift of $z = 0.2$, the duration of the event is greater than one day measured from Earth, although the luminosity of the flare is high only for a few hours. These timescales are proportional to the total mass of the system, so

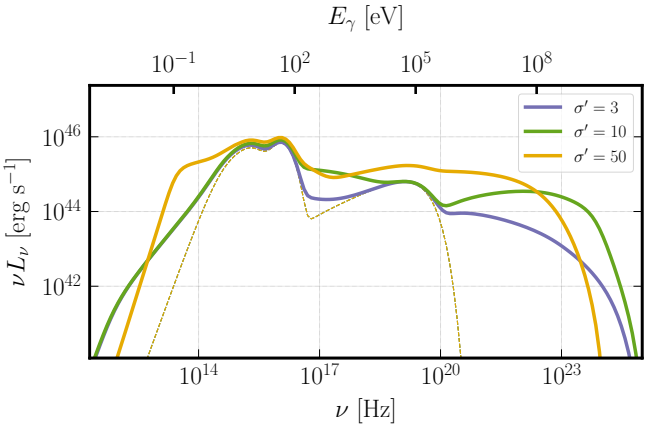

Figure 6. Spectral distribution of energy of the SMBHB in the emission maximum of the jets for different values of the magnetisation. When $\sigma' = 3$, we take $p = 3$, $f_{\rm rec} = 0.15$ and $N_\pm = 1$; when $\sigma' = 10$, we take $p = 2.1$, $f_{\rm rec} = 0.25$ and $N_\pm = 1$; when $\sigma' = 50$, we take $p = 1.5$, $f_{\rm rec} = 0.5$ and $N_\pm = 450$. Dashed lines represent the emission of the discs

that, for the same separation in units of $R_{\rm g}$, the flare can last from a few minutes, if $M \sim 10^5 M_\odot$, up to $\sim$ 50 days, if $M \sim 10^{10} M_\odot$.

3.1.1 Magnetisation

Of the several microphysical parameters of the model, the magnetisation σ' is the most important. The value of the magnetisation determines other relevant microphysical parameters in magnetic reconnection events, such as the maximum (if $\sigma' \gg 1$) and minimum (if $\sigma' \lesssim 10$) energies of the particles (Eqs. 21 and 23), the spectral index of the distribution, p, and the fraction of the reconnected power destined to the non-thermal population, $f_{\rm rec}$. Following the guidelines of Petropoulou et al. (2016), we explore three scenarios of low, medium, and high magnetisation of the jets. These three scenarios are determined by the parameters $(\sigma', p, f_{\rm rec}, N_\pm)$, which take the values $(3, 3, 0.15, 1)$, $(10, 2.1, 0.25, 1)$, and $(50, 1.5, 0.5, 450)$, respectively.The other parameters are fixed to the values of the fiducial model.

Figure 6 shows the SED for these three scenarios. The dotted lines show the emission of the discs, which is independent of magnetisation, while the solid lines correspond to the total emission. The first thing to notice in the image is that the bolometric luminosity of the jets is higher for higher values of σ', since $f_{\rm rec}$ also increases with this parameter. In the high-magnetisation model, the emission is so intense that even in hard X-rays, the jets dominate over the corona.

The SED for low ($\sigma' = 3$) and medium ($\sigma' = 10$) magnetisation are equal to low energies; in these cases $p > 2$ and the minimum energy of the distribution is determined by σ'; however, what determines the lower limit of the distribution is the SSA. On the contrary, in the case of high ($\sigma' = 50$) magnetisation, $p < 2$ holds and the minimum energy is not restricted and can take an arbitrarily small value. However, the emission is strongly self-absorbed below a frequency of $\nu = 10^{13}$Hz.

At high energies, the situation is the reverse of what happens at low energies. For $\sigma' = 50$, the maximum energy of the particle distribution is limited by σ' and is lower than the one that the particles can reach in the other two scenarios where the limit is set by the synchrotron losses (this is valid for the acceleration efficiency parameter of $\epsilon_{\rm acc} = 10^5$ that we take). Then, the spectrum for the $\sigma' = 50$ case,

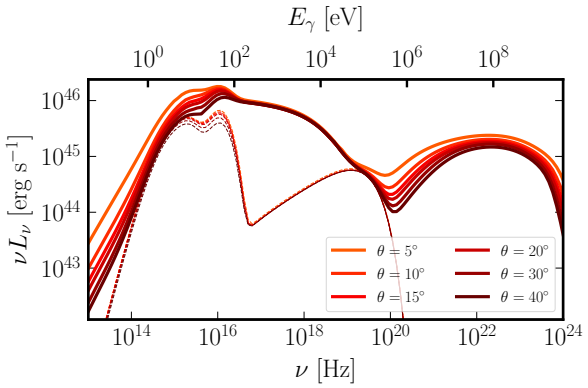

Figure 7. Spectral energy distribution of the SMBHB in the emission maximum of the jets for different values of the spin inclination. Both spins have the same inclination with respect to orbital angular momentum. The other parameters are equal to their values in the fiducial model.

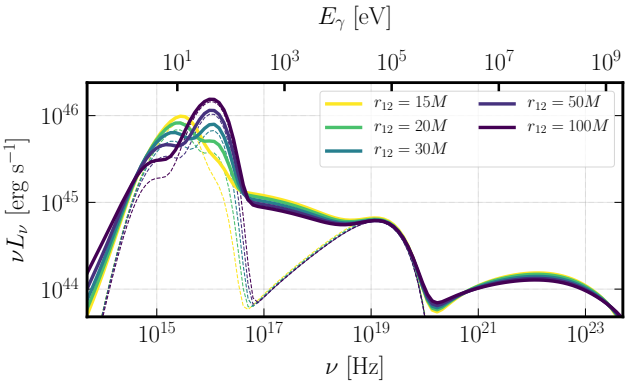

Figure 8. SMBHB spectral energy distribution at the jet emission maximum for different values of black hole separation. We consider models with r_{12} = 15, 20, 30, 50 and 100 R_g. The other parameters are fixed to the values of the fiducial model.

although more intense, decays rapidly above $\sim$ 100 MeV, while in the low and medium magnetisation cases the spectrum reaches slightly higher energies ($\lesssim$ 1GeV). Naturally, the slope of the spectrum in γ rays is steeper for values greater than σ' and less than p.

3.1.2 *Inclination of the spins*

The hypothesis that the spins are tilted is essential for the periodic collisions of the jets to occur. The higher the value of the spins' inclination, $\theta_1 = \theta_2$, the lower the height at which the collision occurs. On the other hand, due to the relativistic movement of the emitting plasma in the jets, their emission is amplified according to the Doppler factor determined by the angle formed by the axis of the jet with the line of sight. To study how the SED changes with spin inclination avoiding changes in the Doppler factor, we fixed in all cases the line of sight in the same direction as the most powerful jet at the moment of the collision.

We vary $\theta_1 = \theta_2$ by taking the values 5°, 10°, 15°, 20°, 30° and 40°. The results are shown in Figure 7. Once again, the SED of the discs is plotted in dotted lines, which now decreases in luminosity for greater spin inclinations, because although one of the discs is always seen face-on, the other is seen more and more edge-on, decreasing its luminosity. In the same way, the CBD looks more edge-on as i increases along with the tilt of the spins.

The jets' SEDs are practically the same in all cases between energies of $\sim$ 100 eV and $\sim$ 100 keV, but they differ both at low and high energies. In both limits, the emission grows inversely with the spin inclination. This is because at low inclinations, the emission of *both* jets is amplified by relativistic Doppler beaming, so both contribute to the SED. At higher tilts, while one of the jets is pointing towards the viewer, the other becomes de-beamed and does not contribute to the SED. Additionally, at low energies the absorption is lower and the luminosity higher for lower inclinations, since the collision occurs at higher altitudes where the magnetic field and particle density are lower. The radio emission then persists down to lower frequencies without being self-absorbed.

3.1.3 *Binary separation*

Another important parameter is the separation of the black holes, r_{12}. At larger separations, the speed of the black holes is lower and also the accretion rate from the mini-discs is less modulated. In turn, these

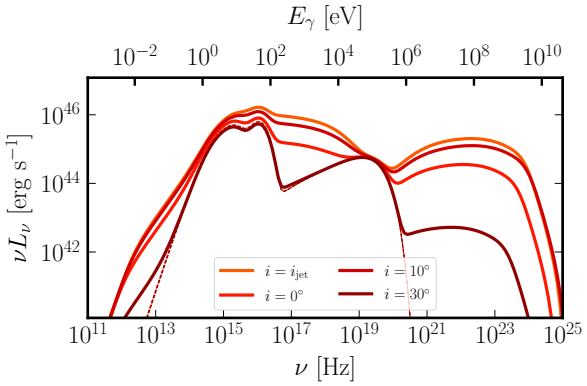

Figure 9. Spectral energy distribution of the SMBHB in the emission maximum of the jets for different values of the inclination of the line of sight. The other parameters are equal to their values in the fiducial model.

are brighter than at short separations, since *a)* the ratio $r_{\rm trunc}/r_{\rm ISCO}$ is greater, and *b)* the accretion time increases so a larger fraction of the mini-disc is thermalised. On the other hand, the further apart the black holes are, the higher the height at which the jets collide. We consider five scenarios with separations r_{12} = 15, 20, 30, 50 and 100 R_g.

The results are shown in Figure 8. Now, the main difference between the various SEDs is the emission from the discs. The greater the separation of the black holes, the dimmer the CBD and the brighter the mini-discs, as they look more and more like regular (dual) AGNs. The SEDs of the jets are very similar for all separations, except for the radio band where the emission is less absorbed the higher the collision occurs (see Sec. 3.1.2), and this increases with the black hole separation.

3.1.4 *Inclination of the line of sight*

We now explore the dependence of the SED with the line of sight inclination with respect to the orbital angular momentum of the SMBHB. We consider scenarios with slopes of $i = 0°$, $i = 10°$, $i = 30°$ and $i = \theta_1$, leaving the other parameters fixed to the values of the fiducial model . Figure 9 shows the results for these scenarios.

The inclination of the line of sight modifies the emission of the discs by two effects: *a)* the greater the inclination, the smaller the

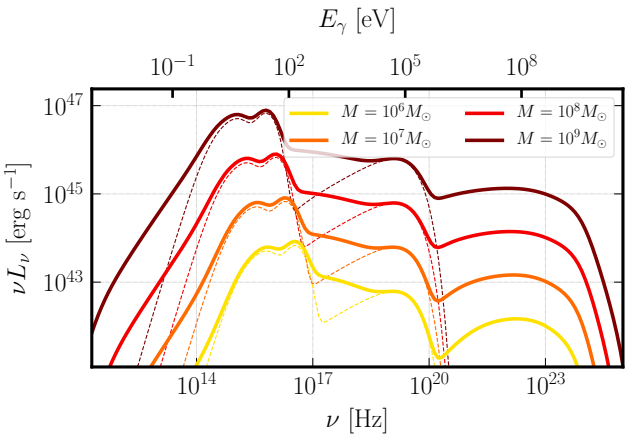

Figure 10. Spectral energy distribution of the SMBHB in the emission maximum of the jets for different values of the total mass $M = m_1 + m_2$. We consider models with $M = 10^6$, 10^7, 10^8 and 10^9. The other parameters are fixed to the values of the fiducial model.

effective surface of the discs, and *b)* the closer to the case edge-on is the line of sight, the greater the effect of relativistic beaming (amplification or decrease) that the mini-discs can suffer. The observed luminosity of the jets strongly depends on the value of the Doppler factor. For the Lorentz factor $\Gamma_j = 5$ that we consider for the jets, the maximum Doppler factor (for $i = \theta_j$) is ≈ 10, so the luminosity of the jet in this case is amplified by a factor $\approx 10^4$.

In Figure 9, the SED for the case $i = \theta_j$ is the brightest, closely followed by our fiducial SED for a tilt $i = 0°$. In this last case, the luminosity of one of the jets is less amplified but that of the other is more. The luminosity of the jets decreases strongly for higher values of the inclination and only contributes slightly in γ rays for $i = 30°$, where $\mathcal{D}_j \approx 1$.

3.1.5 *Total mass of the system*

Finally, we show in Figure 10 the dependence of the SED on the total mass of the system. The bolometric luminosity of the SED is proportional to M. Additionally, the higher the mass, the lower the frequency of SSA so the emission persists down to lower energies. Finally, the thermal peak of the discs scales as $M^{-1/4}$.

3.2 Lightcurves

The main novelty of the emission of the interacting jets in our model is the production of periodic flares. As we saw in the previous Section, at peak emission the luminosity of the jets can exceed that of the accretion discs in certain bands of the electromagnetic spectrum. Furthermore, in the radio and γ-ray bands the discs do not radiate, so only the emission of the jets is visible.

Figure 11 shows light curves at different frequencies for our fiducial model. The upper panel shows the luminosity in the far UV ($\lambda = 30$nm) and in X-rays ($E = 4$keV). At these frequencies, the stationary emission is dominated by the discs, so it is modulated by the variation in the accretion rate with a frequency $2f_{\rm beat}$ (see Sec. 2.2). Superposed with this quasi-sinusoidal light curve, the periodic flashes produced in each collision of the jets are observed with a frequency $f_{\mathcal{B}}$. The maximum luminosity of the flares is also modulated by the filling-depleting cycle just like the discs. The flare profile itself does not provide relevant information since it is determined ad-hoc by the prescription we use to model the power transferred to particles during reconnection (see Sec. 2.4).

The lower panel of Figure 11 shows the luminosity in the millimetre radio band ($\lambda = 1.3$mm) and in soft γ rays ($E = 100$MeV). In these energy bands, the emission from the discs is negligible, so the lightcurve only shows the intense flares caused by the collision between the jets.

If we observe the system with a non-zero inclination with respect to the orbital axis, the emission of the mini-discs will present an additional modulation due to the effect of relativistic beaming (Eq. 8). This effect induces additional sinusoidal variability in the luminosity of the mini-discs, with a slightly higher frequency than that caused by the filling-depleting cycle: $f_{\rm beaming} = 2f_{\mathcal{B}}$ versus $2f_{\rm beat} \approx 1.4 f_{\mathcal{B}}$ (provided both discs shine comparably). The superposition of these two periodic effects converges in a wave of frequency $\approx 2f_{\rm beat}$ modulated by an oscillation of frequency $\approx 0.25 f_{\mathcal{B}}$.

The Doppler factor of the mini-discs will be greater the smaller the separation of the black holes because they will move faster. Then, to better visualise this effect, we consider a separation of $r_{12} = 20R_g$ and plot in Figure 12 the lightcurves in the UV for different inclinations $i = 10°$, $20°$, $30°$, $40°$, $60°$, and $90°$. The emission of the jets is only visible for low inclinations, since we have kept the directions of the spins fixed at $10°$ from the orbital axis. The greater the inclination of the line of sight, the greater the modulation by beaming, so that the maximum of the oscillations reaches higher values. In turn, the envelope modulation that is formed by the combination of the two effects is seen more clearly for higher slopes. The dotted line shows the emission from the mini-discs if the accretion rate were constant; that is, with a modulation only due to *beaming*.

4 DISCUSSION AND CAVEATS OF THE MODEL

In Sec. 3.1, we have presented theoretical predictions for the emission produced in SMBHB in the relativistic regime. The novel theoretical prediction of our model is that of the occurrence of periodic flares caused by the collision of the magnetically-dominated jets launched by SMBHBs.

The flares are produced by relativistic electrons accelerated by magnetic reconnection in the collision region of the jets. The emitted spectrum occupies a broad range in the electromagnetic spectrum. Between infrared and hard X-ray energies, the emission from the CBD and the mini-discs is generally dominant, although during the flares the emission from the jets may overcome the discs' in some bands. At these energies, the flares could be detected in the lightcurves as periodic spikes of different intensities occurring on a sinusoidal oscillatory background. This phenomenology is similar to that of flares produced by other processes such as self-lensing. In this latter case, the emission of the flares is the same emission of the mini-discs but amplified by relativistic effects. Here, on the contrary, the flares have a different origin, in the jet, which will be less correlated with the emission of the discs (and with a time delay). Furthermore, due to their non-thermal origin, the flares from jet collisions radiate at energies below the far infrared as well as at γ rays above the MeV, where discs are not expected to radiate thermally. Then, a way to contrast the origin of flares of this type could be through the identification of the event in the γ-ray band, for example by means of the LAT instrument of the Fermi satellite[5]. Single BH AGNs can also exhibit high-energy emission with high variability from plasmoid

[5] https://fermi.gsfc.nasa.gov/

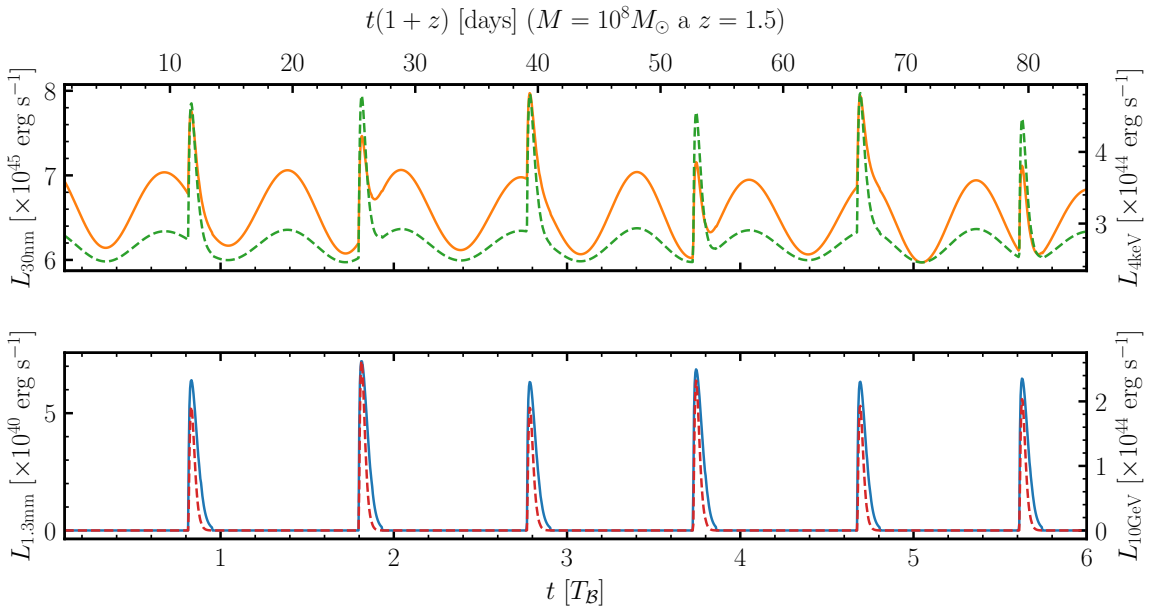

Figure 11. Light curves for the fiducial model. *Upper panel*: Luminosity in the far UV (λ = 30nm), with a solid line, and in X-rays (E = 4keV), with a dashed line. *Lower panel:* Luminosity at λ = 1.3mm, with solid lines, and in γ rays (E = 100MeV), with dashed lines.

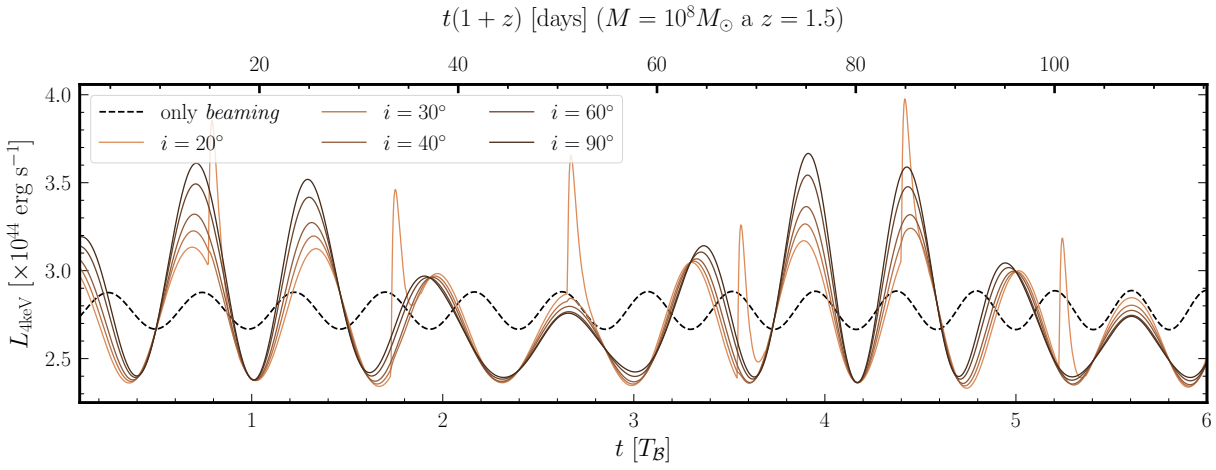

Figure 12. Lightcurves for different line of sight inclinations. The other parameters are those of the fiducial model, except for the separation of the black holes, which here is $r_{12} = 20R_g$.

generation near the BH horizon (Crinquand et al. 2021), and also blazar emission. These mechanisms, however, will produce radiation at energies greater than $\approx$ 100 GeV, which is typically above our estimations for the flux.

In the following sections, we discuss the limitations of our model, open questions, and possible directions in which it can be improved.

4.0.1 Dynamical features of the binary and its accretion

As we have seen, SMBHBs are dynamically very complex systems. This complexity translates into a wide variety of possible associated electromagnetic signals. In this paper, we have proposed that periodic flares of radiation could be produced in the interactions between the jets launched by both black holes. In our treatment, we have also included the emission of CBDs and mini-discs, but not that of streams. As shown in Gutiérrez et al. (2022), the emission of the streams may be significant for separations of $\sim 20R_g$. For the mini-discs, we took into account the quasi-periodic modulation of their luminosity both by the filling-depleting cycle (variable accretion rate) and by the effect of relativistic beaming. To model the properties of these discs, we have used mainly the results of GRMHD simulations (Noble et al. 2012; Bowen et al. 2018; Bowen et al. 2019; Armengol et al. 2021; Noble et al. 2021; Combi et al. 2022; Gutiérrez et al. 2022), since these are the most reliable. However, these simulations are limited to short separations ($r_{12} < 30R_g$), similar masses ($q \sim 1$), and circular orbits. To relax these conditions, it will be necessary to resort to the results of 2D hydrodynamic simulations, which can also provide 'recipes' for semi-analytical modelling the radiation of these systems.

For simplicity, we have considered only leptonic processes in the jet. If protons are accelerated in a similar way to electrons in collision events, they could emit γ radiation by photo-hadronic interaction, as

well as produce neutrinos through the creation and decay of photo-mesons.

On the other hand, there are certain effects that we have not taken into account in our treatment. At the separations considered, if the spins are tilted, they couple with each other and with the orbital angular momentum. This generates a precession of them, which will translate to a precession of the jets. However, for the separations discussed here, the spin precession timescale is $t_{\rm prec} \gg T_{\rm orb}$. The effect of considering the precession will be a delay in the collisions of the jets of approximately $\Delta t_{\rm prec} \sim P_{\rm prec}$ in each orbit, so the flares would be slightly more widely spaced in time.

A precession of the jets would infringe, by itself, a variability in the emission through the variation in the Doppler factor caused by the change in the angle between the line of sight and the axis of the jet (Begelman et al. 1980; O'Neill et al. 2021). Other phenomena that can cause the precession of the jet are *i)* the orbital movement itself that causes non-inertial forces in the plasma of the jet (see Ap. A), *ii*) the Bardeen–Petterson effect, or *iii)* the interaction between the jet and the winds of the discs or even with the other jet. Any of these effects would induce the jets to have a helical structure.

Another effect not considered in our treatment is the deflection of light in the vicinity of black holes. This is of special relevance in SMBHBs because if the system is seen close to edge-on, strong periodic flares can be produced by the self-lensing that occurs when a black hole (and its mini-disc) passes behind the other. In this configuration, the light is focussed towards the observer and the luminosity can be increased by several factors (D'Orazio & Di Stefano 2018; Kelly et al. 2021; Hu et al. 2020; Ingram et al. 2021; Davelaar & Haiman 2022a,b). Finally, we have focused here on the accretion regime of luminous thin discs. The phenomenology may change significantly if the accretion rate is lower and the accretion flow has the properties of a radiatively inefficient hot accretion flow.

4.0.2 Reconnection at the jet-jet collision region

In our model, the outcome of the reconnection event at the collision is simply approximated as the formation of two large blobs travelling along each jet. The formation of a three-dimensional, dynamical current sheet in the jet-jet collision region will produce much more complex phenomena in a regime currently unexplored in PIC simulations. A detailed analysis of plasmoid evolution, which treat individual growth and mergers in a highly dynamic and non-linear environment, is beyond the scope of this work.

Magnetic reconnection in magnetically-dominated plasmas typically produces plasmoids of different sizes. Each of these plasmoids evolves, radiates, and eventually expands and cools completely as it leaves the current sheet (Sironi et al. 2016; Petropoulou et al. 2016, 2018). Different plasmoids will grow to different sizes, the smallest being highly relativistic in the co-moving frame of the jet, $\beta'_{\rm p}\Gamma'_{\rm p} \sim \Gamma'_{\rm p}$, whereas the largest being only slightly relativistic, $\beta'_{\rm p}\Gamma'_{\rm p} \lesssim 1$, where $\beta'_{\rm p}$ is the normalised velocity of the plasmoid in the jet's comoving frame and $\Gamma'_{\rm p} = (1-\beta'^2_{\rm p})^{-1/2}$ is its Lorentz factor. Although we assume that only two giant plasmoids are formed per collision (similarly as in, e.g., Crinquand et al. 2021), the formation of other small relativistic plasmoids might also produce short, intense flares superposed on an enveloping flare produced by the larger plasmoids (e.g., Giannios 2013).

In the highly magnetised region where the jets collide, magnetic reconnection could happen close to the radiative regime where synchrotron cooling dominates over acceleration (Hakobyan et al. 2022). In that case, the plasmoids, which contain the accelerated particles, reduce significantly their size and emit mostly synchrotron radiation (Mahlmann et al. 2022; Hakobyan et al. 2021, 2022). On the contrary, in our model, we considered that we are not in the radiative regime and thus all the high-energy particles are carried by plasmoids. We have also neglected three-dimensional effects, which are just starting to be investigated in PIC and force-free simulations (Zhang et al. 2021) and might bring the current sheet out of our stationary scenario. Finally, in the highly-magnetised fast collisions of the jets, one could speculate on other dissipation mechanisms such as interacting Alfvén waves moving along the jet (Li et al. 2021).

New dynamical MHD simulations of interacting jets in SMBHBs are needed to further understand the properties of the collision event. These simulations could be performed in many different regimes: kinetic, force-free, or ideal MHD, capturing different aspects of the system. Our analytical model is just the first step towards this goal.

5 SUMMARY AND CONCLUSIONS

We have developed for the first time a model to calculate the emission produced by the interaction of two relativistic jets in an SMBHB in the relativistic regime. If the jets are launched with a small inclination with respect to the orbital angular momentum, they may collide with each other. This collision would occur periodically, at an approximate rate of once per orbit. The collision of the magnetised jets at high speeds provides excellent conditions for the development of strong magnetic reconnection events. In this type of event, a fraction of the energy released from the magnetic field is transferred to the particles present in the region, which are accelerated and form a non-thermal distribution. These particles then cool by synchrotron radiation and SSC. Due to the high Lorentz factors that are reached in relativistic jets, the emission of these during the reconnection events can be strongly amplified in the direction of the observer and exceed the luminosity of the CBD and the mini-discs, if the line of sight inclination is favourable. In addition, these events produce emission of electromagnetic radiation in the radio and γ-ray bands, where discs do not emit, so the detection of periodic flares at different frequencies of the spectrum may indicate that they are due to the interaction of jets and discard other effects. In the future, we will study some situations not considered here, such as the case of low mass ratios $q < 1$, eccentric orbits or aligned spins.

ACKNOWLEDGEMENTS

We thank Jens Mahlmann for fruitful discussions about plasmoids and magnetic reconnection physics. We have extensively used the open-source tools provided by `Matplotlib` (Hunter 2007), `NumPy` (Harris et al. 2020), and `SciPy` (Virtanen et al. 2020). E. M. G. and L. C received support from CONICET (Argentina's National Research Council) fellowship program and from the Rochester Institute of Technology's Center for Computational Relativity and Gravitation. LC is a CITA National fellow and acknowledges the support of the Natural Sciences and Engineering Research Council of Canada (NSERC), funding reference DIS-2022-568580. Research at Perimeter Institute is supported in part by the Government of Canada through the Department of Innovation, Science and Economic Development Canada and by the Province of Ontario through the Ministry of Colleges and Universities. Additionally, M.C. gratefully acknowledge support from NSF awards NSF AST-2009330, OAC-2031744 and PHY-1806596, PHY-2110352 and NASA TCAN grant (NNH17ZDA001N). Computational resources

were provided by the TACC's Frontera supercomputer allocation No. PHY-20010 and AST-20021. Additional resources were provided by the RIT's BlueSky and Green Pairie and Lagoon Clusters acquired with NSF grants PHY-2018420, PHY-0722703, PHY-1229173 and PHY-1726215. G.E.R. acknowledges the support by the Spanish Ministerio de Ciencia e Innovación (MICINN) under grant PID2019-105510GB-C31/AEI/10.13039/501100011033 and through the "Center of Excellence María de Maeztu 2020-2023" award to the ICCUB (CEX2019-000918-M) and PIP 0554 (CONICET).

REFERENCES

Alic D., Moesta P., Rezzolla L., Zanotti O., Jaramillo J. L., 2012, The Astrophysical Journal, 754, 36
Armengol F. G. L., et al., 2021, The Astrophysical Journal, 913, 16
Arzoumanian Z., et al., 2020, The Astrophysical journal letters, 905, L34
Bardeen J. M., Petterson J. A., 1975, ApJ, 195, L65+
Begelman M. C., Blandford R. D., Rees M. J., 1980, Nature, 287, 307
Blandford R. D., Znajek R. L., 1977, MNRAS, 179, 433
Bogdanović T., Reynolds C. S., Miller M. C., 2007, ApJ, 661, L147
Bogdanović T., Eracleous M., Sigurdsson S., 2009, ApJ, 697, 288
Bogdanovic T., Miller M. C., Blecha L., 2021, arXiv preprint arXiv:2109.03262
Bowen D. B., Mewes V., Campanelli M., Noble S. C., Krolik J. H., Zilhão M., 2018, The Astrophysical Journal Letters, 853, L17
Bowen D. B., Mewes V., Noble S. C., Avara M., Campanelli M., Krolik J. H., 2019, ApJ, 879, 76
Burke-Spolaor S., et al., 2019, The Astronomy and Astrophysics Review, 27, 5
Campanelli M., Lousto C. O., Zlochower Y., 2006a, Phys. Rev. D, 74, 084023
Campanelli M., Lousto C. O., Zlochower Y., 2006b, Phys. Rev. D, 74, 084023
Cattorini F., Giacomazzo B., Haardt F., Colpi M., 2021, Physical Review D, 103, 103022
Combi L., Lopez Armengol F. G., Campanelli M., Noble S. C., Avara M., Krolik J. H., Bowen D., 2022, ApJ, 928, 187
Crinquand B., Cerutti B., Dubus G., Parfrey K., Philippov A., 2021, Astronomy & Astrophysics, 650, A163
D'Orazio D. J., Di Stefano R., 2018, MNRAS, 474, 2975
D'Orazio D. J., Haiman Z., Duffell P., Farris B. D., MacFadyen A. I., 2015, MNRAS, 452, 2540
Davelaar J., Haiman Z., 2022a, Phys. Rev. D, 105, 103010
Davelaar J., Haiman Z., 2022b, Phys. Rev. Lett., 128, 191101
Dermer C. D., Menon G., 2009, High Energy Radiation from Black Holes: Gamma Rays, Cosmic Rays, and Neutrinos
Dotti M., Montuori C., Decarli R., Volonteri M., Colpi M., Haardt F., 2009, Monthly Notices of the Royal Astronomical Society: Letters, 398, L73
Dotti M., Volonteri M., Perego A., Colpi M., Ruszkowski M., Haardt F., 2010, MNRAS, 402, 682
Engel K., et al., 2022, arXiv preprint arXiv:2203.10074
Falcke H., Biermann P. L., 1995, A&A, 293, 665
Farris B. D., Gold R., Paschalidis V., Etienne Z. B., Shapiro S. L., 2012, Phys. Rev. Lett., 109, 221102
Frank J., Rees M. J., 1976, Monthly Notices of the Royal Astronomical Society, 176, 633
Gerosa D., Veronesi B., Lodato G., Rosotti G., 2015, MNRAS, 451, 3941
Gerosa D., Rosotti G., Barbieri R., 2020, MNRAS, 496, 3060
Giacomazzo B., Baker J. G., Miller M. C., Reynolds C. S., van Meter J. R., 2012, The Astrophysical Journal Letters, 752, L15
Giannios D., 2013, MNRAS, 431, 355
Gold R., Paschalidis V., Etienne Z. B., Shapiro S. L., Pfeiffer H. P., 2014a, Physical Review D, 89
Gold R., Paschalidis V., Ruiz M., Shapiro S. L., Etienne Z. B., Pfeiffer H. P., 2014b, Physical Review D, 90
Gold R., Paschalidis V., Ruiz M., Shapiro S. L., Etienne Z. B., Pfeiffer H. P., 2014c, Phys. Rev. D, 90, 104030
Graham M. J., et al., 2015a, Monthly Notices of the Royal Astronomical Society, 453, 1562
Graham M. J., et al., 2015b, Nature, 518, 74
Guo F., Li H., Daughton W., Liu Y.-H., 2014, Phys. Rev. Lett., 113, 155005
Guo F., Liu Y.-H., Daughton W., Li H., 2015, ApJ, 806, 167
Guo F., et al., 2016, ApJ, 818, L9
Guo F., Li X., Daughton W., Li H., Kilian P., Liu Y.-H., Zhang Q., Zhang H., 2021, ApJ, 919, 111
Gutiérrez E. M., Combi L., Noble S. C., Campanelli M., Krolik J. H., López Armengol F., García F., 2022, ApJ, 928, 137
Hakobyan H., Petropoulou M., Spitkovsky A., Sironi L., 2021, The Astrophysical Journal, 912, 48
Hakobyan H., Ripperda B., Philippov A., 2022, arXiv preprint arXiv:2209.02105
Harris C. R., et al., 2020, Nature, 585, 357
Hu B. X., D'Orazio D. J., Haiman Z., Smith K. L., Snios B., Charisi M., Di Stefano R., 2020, MNRAS, 495, 4061
Hunter J. D., 2007, Computing in Science & Engineering, 9, 90
Ingram A., Motta S. E., Aigrain S., Karastergiou A., 2021, Monthly Notices of the Royal Astronomical Society, 503, 1703
Jiang N., et al., 2022, arXiv preprint arXiv:2201.11633
Kelley L. Z., Blecha L., Hernquist L., 2017, MNRAS, 464, 3131
Kelly B. J., Baker J. G., Etienne Z. B., Giacomazzo B., Schnittman J., 2017, Phys. Rev. D, 96, 123003
Kelly B. J., Etienne Z. B., Golomb J., Schnittman J. D., Baker J. G., Noble S. C., Ryan G., 2021, Phys. Rev. D, 103, 063039
King A. R., Lubow S. H., Ogilvie G. I., Pringle J. E., 2005, MNRAS, 363, 49
Kormendy J., Ho L. C., 2013, ARA&A, 51, 511
Kormendy J., Richstone D., 1995, Annual Review of Astronomy and Astrophysics, 33, 581
Kumar S., Pringle J. E., 1985, MNRAS, 213, 435
Lense J., Thirring H., 1918, Physikalische Zeitschrift, 19, 156
Li X., Beloborodov A. M., Sironi L., 2021, The Astrophysical Journal, 915, 101
Liska M., Tchekhovskoy A., Ingram A., van der Klis M., 2019, MNRAS, 487, 550
Liska M., Hesp C., Tchekhovskoy A., Ingram A., van der Klis M., Markoff S. B., Van Moer M., 2021, MNRAS, 507, 983
Liu T., et al., 2019, The Astrophysical Journal, 884, 36
Lodato G., Gerosa D., 2013, MNRAS, 429, L30
Lodato G., Price D. J., 2010, MNRAS, 405, 1212
Lodato G., Pringle J. E., 2007, MNRAS, 381, 1287
Lopez Armengol F. G., et al., 2021, arXiv e-prints, p. arXiv:2102.00243
MacFadyen A. I., Milosavljević M., 2008, ApJ, 672, 83
Magorrian J., et al., 1998, The Astronomical Journal, 115, 2285
Mahlmann J., Philippov A., Levinson A., Spitkovsky A., Hakobyan H., 2022, arXiv preprint arXiv:2203.04320
Mangiagli A., Caprini C., Volonteri M., Marsat S., Vergani S., Tamanini N., Inchauspé H., 2022, arXiv preprint arXiv:2207.10678
McWilliams S. T., Ostriker J. P., Pretorius F., 2014, The Astrophysical Journal, 789, 156
Melzani M., Walder R., Folini D., Winisdoerffer C., Favre J. M., 2014, A&A, 570, A112
Merritt D., Milosavljević M., 2005, Living Reviews in Relativity, 8, 8
Mezcua M., 2017, International Journal of Modern Physics D, 26, 1730021
Miller M. C., Krolik J. H., 2013, ApJ, 774, 43
Milosavljević M., Merritt D., 2003, in AIP Conference Proceedings. pp 201–210
Milosavljević M., Phinney E. S., 2005, ApJ, 622, L93
Moesta P., Alic D., Rezzolla L., Zanotti O., Palenzuela C., 2012, The Astrophysical Journal Letters, 749, L32
Mösta P., Palenzuela C., Rezzolla L., Lehner L., Yoshida S., Pollney D., 2010, Phys. Rev. D, 81, 064017
Natarajan P., Pringle J. E., 1998, ApJ, 506, L97
Nealon R., Ragusa E., Gerosa D., Rosotti G., Barbieri R., 2022, MNRAS, 509, 5608
Nelson R. P., Papaloizou J. C. B., 2000, MNRAS, 315, 570

Noble S. C., Mundim B. C., Nakano H., Krolik J. H., Campanelli M., Zlochower Y., Yunes N., 2012, The Astrophysical Journal, 755, 51
Noble S. C., Krolik J. H., Campanelli M., Zlochower Y., Mundim B. C., Nakano H., Zilhão M., 2021, arXiv preprint arXiv:2103.12100
O'Neill S., et al., 2021, arXiv e-prints, p. arXiv:2111.02436
Palenzuela C., Anderson M., Lehner L., Liebling S. L., Neilsen D., 2009, Physical Review Letters, 103, 081101
Palenzuela C., Lehner L., Yoshida S., 2010a, Physical Review D, 81, 084007
Palenzuela C., Garrett T., Lehner L., Liebling S. L., 2010b, Phys. Rev. D, 82, 044045
Palenzuela C., Lehner L., Liebling S. L., 2010c, Science, 329, 927
Paschalidis V., Bright J., Ruiz M., Gold R., 2021a, ApJ, 910, L26
Paschalidis V., Bright J., Ruiz M., Gold R., 2021b, ApJ, 910, L26
Perego A., Dotti M., Colpi M., Volonteri M., 2009, MNRAS, 399, 2249
Peters P. C., 1964, Phys. Rev., 136, B1224
Petropoulou M., Giannios D., Sironi L., 2016, MNRAS, 462, 3325
Petropoulou M., Christie I. M., Sironi L., Giannios D., 2018, MNRAS, 475, 3797
Petropoulou M., Sironi L., Spitkovsky A., Giannios D., 2019, ApJ, 880, 37
Quinlan G. D., 1996, New Astronomy, 1, 35
Reines A. E., Greene J. E., Geha M., 2013, The Astrophysical Journal, 775, 116
Roedig C., Krolik J. H., Miller M. C., 2014, ApJ, 785, 115
Saade M. L., et al., 2020, arXiv e-prints, p. arXiv:2001.08870
Samtaney R., Loureiro N. F., Uzdensky D. A., Schekochihin A. A., Cowley S. C., 2009, Phys. Rev. Lett., 103, 105004
Sesana A., Gualandris A., Dotti M., 2011, MNRAS, 415, L35
Shakura N. I., Sunyaev R. A., 1973, A&A, 24, 337
Sironi L., Spitkovsky A., 2011, ApJ, 741, 39
Sironi L., Spitkovsky A., 2014, ApJ, 783, L21
Sironi L., Petropoulou M., Giannios D., 2015, MNRAS, 450, 183
Sironi L., Giannios D., Petropoulou M., 2016, MNRAS, 462, 48
Small T. A., Blandford R. D., 1992, Monthly Notices of the Royal Astronomical Society, 259, 725
Soltan A., 1982, MNRAS, 200, 115
Uzdensky D. A., Loureiro N. F., Schekochihin A. A., 2010, Phys. Rev. Lett., 105, 235002
Valtonen M. J., et al., 2006, ApJ, 643, L9
Valtonen M. J., et al., 2008, Nature, 452, 851
Vasiliev E., Antonini F., Merritt D., 2015, ApJ, 810, 49
Virtanen P., et al., 2020, Nature Methods, 17, 261
Werner G. R., Uzdensky D. A., Cerutti B., Nalewajko K., Begelman M. C., 2016, ApJ, 816, L8
Zenitani S., Hoshino M., 2001, ApJ, 562, L63
Zhang H., Sironi L., Giannios D., 2021, The Astrophysical Journal, 922, 261
d'Ascoli S., Noble S. C., Bowen D. B., Campanelli M., Krolik J. H., Mewes V., 2018, ApJ, 865, 140

APPENDIX A: BENDING OF THE JETS BY INERTIAL FORCES

We have modelled the jets as magnetically rigid plasmas, each pointing in the direction of the spin of the black hole from which they are ejected. The actual situation appears to be much more complex than this since the reference frames of the black holes are not inertial. Black holes move in circular Keplerian orbits with orbital velocity $\sim (r_{12}/R_{\rm g})c$. In the rotating frame that follows a given black hole, a given portion of plasma in the jet will be subjected to an outwards centrifugal force and a Coriolis force pointing in the direction of the black hole's motion. The collective effect of these inertial forces pointing in different directions along the orbit of the holes results in bent jets that will have a helical structure.

If the centrifugal force is strong enough, the jets can quickly twist outwards and never encounter each other. To estimate the relative importance of the centrifugal force, we write the equation of motion for a jet particle in the r direction in the co-rotating reference frame with the black hole:

$$\ddot{r} = \Omega_{\mathcal{B}}^2 r. \tag{A1}$$

We can impose an upper limit on the importance of the centrifugal force by replacing the right-hand side of Eq. A1 with $\Omega_{\mathcal{B}}^2(r_{12}/2)$, which corresponds to the maximum centrifugal force felt by a particle of the jet that is initially thrown towards the centre. If the jet has an inclination θ with respect to the angular momentum vector of the binary, the initial velocity of the jet particle in the direction r is $\sim -\beta_{\rm j} c\, sin\theta$ and the solution of Eq. A1 is

$$r(t) = \frac{\Omega_{\mathcal{B}}^2 r_{12}}{4} t^2 - \beta_{\rm j} c \sin\theta t + r_{12}/2. \tag{A2}$$

The relationship between the first and second terms in the above equation gives an estimate of the relevance of the centrifugal force:

$$\left|\frac{\Delta r_{\rm c}}{\Delta r_{\rm i}}\right| \sim \frac{\Omega_{\mathcal{B}}^2 r_{12}}{4\beta_{\rm j} c \sin\theta} \Delta t. \tag{A3}$$

We require this ratio to be small for the time it takes for a particle in the jet to reach the collision region.

Assuming similar conditions for both jets, the collision occurs at $r \sim 0$, $\tilde{z} \sim r_{12}/2 \sin\theta$, and then $\Delta t \sim \tilde{z}/\beta_{\rm j} c \sim r_{12}/2 \sin\theta \beta_{\rm j} c$. Substituting this into Eq. A3, we get

$$\left|\frac{\Delta r_{\rm c}}{\Delta r_{\rm i}}\right| \sim \frac{1}{8(r_{12}/r_{\rm g})\beta_{\rm j}^2 \sin^2\theta}, \tag{A4}$$

and so, for $\theta \gtrsim 10°$, $|\Delta r_{\rm c}/\Delta r_{\rm i}| \lesssim 10^{-1}$, and we can reasonably ignore the effect of centrifugal force for our purposes.

The Coriolis force is less of a problem since the twist it produces in the jets is in the direction of the black hole's motion but not outwards (in the co-rotating frame). Then this force will change the orbital phase in which the jets interact, but it will not prevent the periodic interaction.